Spongelike Rigid Structures in Frictional Granular Packings

Kuang Liu[®], ¹ Jonathan E. Kollmer[®], ^{2,3} Karen E. Daniels[®], ³ J. M. Schwarz[®], ^{1,4} and Silke Henkes[®] ¹ Physics Department, Syracuse University, Syracuse, New York 13244, USA ² Experimental Astrophysics, Department of Physics, Universität Duisburg-Essen, Lotharst. 1, 47057 Duisburg, Dortmund, Germany ³ Department of Physics, North Carolina State University, 27695 Raleigh, North Carolina, USA ⁴ Indian Creek Farm, Ithaca, New York 14850, USA ⁵ School of Mathematics, University of Bristol, BS8 1UG Bristol, England, United Kingdom

(Received 30 May 2020; revised 12 November 2020; accepted 30 November 2020; published 22 February 2021)

We show how rigidity emerges in experiments on sheared two-dimensional frictional granular materials by using generalizations of two methods for identifying rigid structures. Both approaches, the force-based dynamical matrix and the topology-based rigidity percolation, agree with each other and identify similar rigid structures. As the system becomes jammed, at a critical contact number $z_c = 2.4 \pm 0.1$, a rigid backbone interspersed with floppy, particle-filled holes of a broad range of sizes emerges, creating a spongelike morphology. While the pressure within rigid structures always exceeds the pressure outside the rigid structures, they are not identified with the force chains of shear jamming. These findings highlight the need to focus on mechanical stability arising through arch structures and hinges at the mesoscale.

DOI: 10.1103/PhysRevLett.126.088002

Rigidity is the ability of a system to resist imposed perturbations; for disordered materials, their detailed internal structure determines rigidity [1,2]. The Maxwell counting criterion [3], first developed for building girder frameworks in 19th century railway bridges, has long been used to compute the stability of the system by comparing the number of constraints to the number of degrees of freedom [4]. This simple, effectively mean-field, criterion correctly predicts the onset of positive bulk and shear moduli in frictionless jamming of spherical particles (e.g., foams or emulsions) [5–8]. However, when friction is introduced, the counting argument no longer works, even with modifications [9–11], suggesting that one must go beyond mean-field constraint counting to understand frictional rigidity. In particular, systems that acquire rigidity under shear do so at lower packing fractions than those loaded isotropically, via the appearance of anisotropic, load-bearing force chains, in a phenomenon known as shear jamming [11,12].

A first approach to local rigidity, linear response theory, uses the detailed local geometry and forces to compute the *dynamical matrix* or Hessian of the system [13]. Rigid packings have no system-spanning zero modes in the dynamical matrix, except for global translations and rotations; conversely, their presence indicates a lack of rigidity. In frictionless systems, this method agrees with the result of Maxwell constraint counting, after removing so-called "rattlers" (isolated particles) [13]. In frictional systems, the same comparison was made using a dynamical matrix extended to include friction [14,15]. In frictional simulations equilibrated at constant pressure, results agree with a

generalised form of constraint counting, creating a frictional jamming transition along a generalized isostaticity line [10,15]. Other modified frictional isostatic conditions have been proposed [16,17], but none have yet been experimentally tested.

A second approach to quantifying local rigidity focuses on the spatial patterns of rigid clusters: sets of connected bonds that are mutually rigid [18]. Rigidity percolation corresponds to the emergence of a spanning rigid cluster in the contact network. In two dimensions and with central-force interactions, there exists a generic algorithm for decomposing a network *graph* into rigid clusters and floppy regions, the *pebble game* [19], independent of forces and contact geometry. Analysis of 2D frictionless packings recently showed that they exhibit a discontinuous rigidity transition [20], while generic central-force spring networks exhibit a continuous transition [21,22]. Rigidity percolation has also provided insights into the structure of colloidal gels with attractive interactions [23–25].

Recent work [26] generalizes rigidity percolation to include friction by extending the pebble game to frictional packings and shows that networks derived from slowly sheared frictional simulations generate rigid cluster structures consistent with a continuous transition. A simplified lattice model with friction provides further support for a second-order frictional rigidity transition in its own universality class [27]. Recent work on frictional packings numerically generated from frictionless simulations links the onset of shear jamming to the percolation of overconstrained regions [28] and finds correlations between the

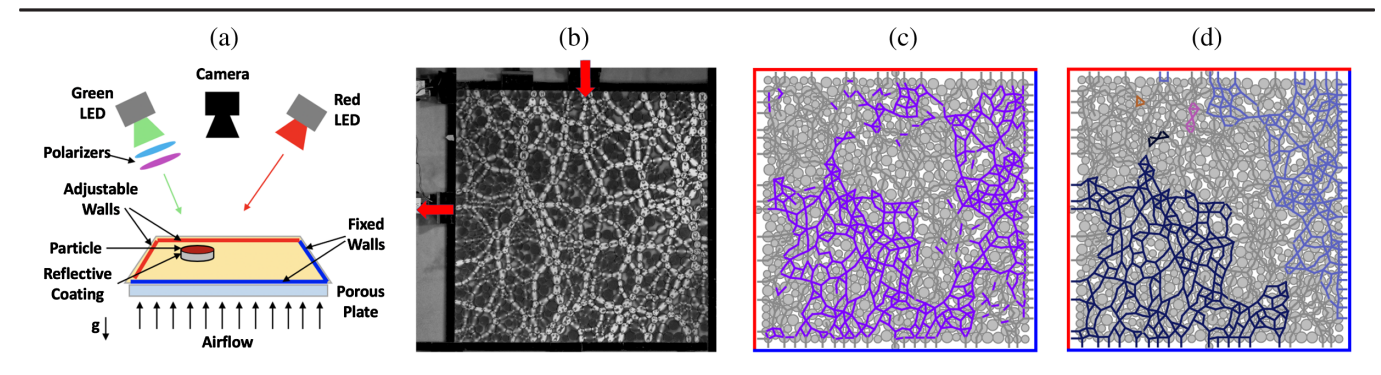


FIG. 1. (a) Schematic of the experimental setup with fixed walls (blue) and moving walls (red). (b) Sample image, showing just the polarized channel (photoelastic respose). (c) Rigid region decomposition of sample (b), computed using the dynamical matrix; the rigid region is purple, and floppy bonds are gray. (d) Rigid cluster decomposition of sample (b), computed using the pebble game; it contains two large rigid clusters (blue and red bonds), some smaller rigid clusters (other colors), and regions of floppy bonds (grey). Colors simply label distinct clusters, and have no other significance.

rigid structures and force-chain percolation, the shear jamming measure [11,12].

In this Letter, we remedy the lack of experimental tests of constraint counting and apply both the dynamical matrix and the pebble game to data from experiments on 2D frictional granular packings. We measure particle positions and forces within a monolayer of quasistatically sheared disks floating on a gentle cushion of air [29,30], with interparticle forces obtained using photoelasticity [31,32]. We find that the frictional dynamical matrix and the frictional pebble game provide nearly identical decompositions of the packings into rigid and floppy regions, and that there is a strong correlation between local pressure and local rigidity. In contrast, while our system shear jams, we find no correlation between force chains and rigid clusters. The transition in our finite-sized system occurs at $z_c = 2.4 \pm 0.1$, well below the mean field value $z_c = 3$. We discover that the rigid structures are spongelike, i.e., containing a broad range of floppy hole sizes, another signature of a continuous transition inconsistent with meanfield rigidity.

Experiments.— We perform experiments on a monolayer of N = 826 photoelastic bidisperse disks [Fig. 1(a)]. The two particle radii are $R_1 = 5.5$ and $R_2 = 7.7$ mm (with $R_2/R_1 = 1.4$), and the particles are initially confined to an area of approximately $L = 0.5 \times 0.5 \text{ m}^2$. Two of the confining walls are controlled by stepper motors; to impose pure shear, one wall moves in while the other moves out in a series of quasistatic steps of size $\Delta x = 1.5$ mm, with Δy adjusted to maintain constant area A. After n steps, each resulting in a shear strain $\epsilon = \Delta x/L \approx 0.003$, the shear is reversed back to the initial state. The number of steps is not fixed, but ranges from n = 8 (ending at a total stress threshold) to n = 13 (predefined maximum). The floor of the shear cell is a porous frit through which air flows to allow the particles to float on a gentle air cushion, creating a system without basal friction; this apparatus is largely the same as the one described in Refs. [29,30]. Therefore, the external load from the two walls is the only significant external stress. The complete dataset consists of 24 cyclic runs, with each run starting from randomized particle positions and an initial barely jammed volume. The packing fraction for each of the 24 runs is in the range $0.746 < \phi < 0.760 \pm 0.006$. During each cycle, contacts are created through shear during the first half of the cycle (dubbed "shear"), and partially released during the second half of the cycle (dubbed "unshear"); due to shear jamming [11,33], the system does not return to its initial state after a complete cycle. Datasets where we could not track all particles where discarded. A total of 353 images are used in the analysis below. Since the particles are made of a birefringent material (Vishay PhotoStress PSM-4), we are able to use photoelasticity [31,32] to measure the vector contact forces on all particles; a sample image is shown in Fig. 1(b). The red channel (not shown) uses unpolarized light and measures particle positions, and the green channel (shown) uses circularly polarized light to measure the photoelastic signal. From the latter, we determine the normal and tangential contact forces $(f_n,$ f_t) on each particle using our open-source algorithms [31,34]. From measurements of the normal f_n and tangential f_t contact forces, we estimate a friction coefficient of $\mu = 0.3$ (see Ref. [35]). The Coulomb threshold for the mobilization $m = |f_t|/\mu f_n$ divides contacts into sliding $(m \ge 1)$ or frictional (m < 1); its experimental distribution is complex (see Fig. D14 in Ref. [35]) and P(m) has so far only been analysed in simulations [10]. The rigidity calculations, described below, depend sensitively on the correct determination of whether two particles are in contact. The Supplemental Material [35] provides information on how we determine the optimal parameters. In all cases, we find that values of the mean coordination number are known to within ± 0.1 .

Rigidity computations.—We first compute the vibrational modes of the system, starting by expanding the equations of motion about mechanical equilibrium

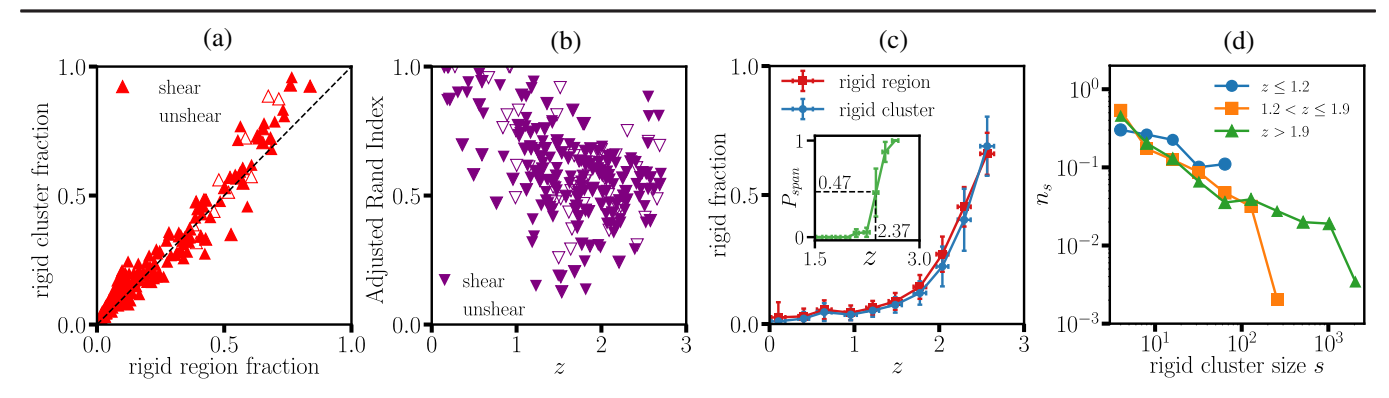


FIG. 2. Correlations between rigid clusters and regions, calculated on the 353-image dataset. (a) Correlation between the rigid cluster fraction and the rigid region fraction. (b) ARI between the rigid cluster decomposition and the rigid region decomposition. (c) Fractions of rigid clusters and rigid regions as function of average coordination number, z. Inset: Probability of a spanning rigid cluster, defining z_c . (d) Histogram of cluster size s, taken for three different ranges of z.

$$\delta \ddot{r}^i_{\alpha} = -D^{ij}_{\alpha\beta} \delta r^j_{\beta} + \text{dissipation}(\delta \dot{r}) + O(\delta r^2),$$
 (1)

where $D_{\alpha,\beta}^{ij}=(1/\sqrt{m_{i,\alpha}m_{j,\beta}})[(\partial^2 V_{ij})/(\partial r_{i,\alpha}r_{j,\beta})]$ is the dynamical matrix of the system, the indices (i,j) label all disks, (α,β) label the two spatial x,y components and the angular component $R\theta$, and m denotes the particle mass. While frictional interactions are not conservative, one can nevertheless derive an effective potential in linear response (see Ref. [35]). We arrive at $V_{\rm eff}^f=\frac{1}{2}K_t\delta t^2$ for a contact with stiffness K_t during tangential contact loading, where δt is the tangential displacement at the contact point. For a sliding contact at the Coulomb threshold, we approximate that the shear dynamics does not reverse the sliding direction. We have verified this assumption in sheared simulations [36] and do not include the shear-reversal step in our analysis here. We obtain $V_{\rm eff}^f=\pm \mu f_n\delta t$, where f_n is the value of the normal force at equilibrium. Then the effective potential becomes [14,15,35]

$$V_{ij} = \frac{1}{2} [K_n (\delta \mathbf{r} \cdot \hat{\mathbf{n}})^2 - f_n / |\mathbf{r}_{ij}| (\delta \mathbf{r} \cdot \hat{\mathbf{t}})^2 + V_{\text{eff}}^f], \quad (2)$$

with normal elastic stiffness K_n , and where the third term arises only for friction. To construct the dynamical matrix for our experimental data, we use measured masses for m, and estimate K_n from the elastic modulus of the material and we approximate $K_t = K_n$. Using the particle positions and interparticle forces, we then construct the dynamical matrix and compute its normalized eigenmodes. The zero eigenvalue modes parametrize the floppy motions, and we determine the translational and rotational relative displacements at all contacts. We then compute the mean square displacement over floppy modes at individual bonds and mark all bonds with a displacement below (above) a threshold value 2×10^{-5} as rigid (floppy); there is mild threshold dependence [35]. In the transition region, we obtain sets of contiguous rigid bonds that form rigid regions, shown in Fig. 1(c).

Our second method of measuring rigidity is to decompose the system into rigid clusters using the frictional pebble game. To do so, we extend the central force (k =2, l = 3) pebble game applied to a contact network to a (k = 3, l = 3) pebble game in order to incorporate the additional rotational degree of freedom made relevant by the friction between disks. Moreover, each contact below the Coulomb threshold contributes two constraints (one normal and one tangential), while each contact at the threshold (freely sliding) only contributes a normal constraint. To this constraint network, we add an appropriate number of constraint bonds between the four boundaries in the experiment and all contacting particles. Please see the Supplemental Material [35], which also includes Refs. [37– 44], and Refs. [26,27] for details. A sample decomposition is shown in Fig. 1(d).

Results.—Using the particle positions and interparticle forces obtained from experiments, we apply the dynamical matrix method and the frictional pebble game to determine rigid regions and rigid clusters, respectively. Figures 1(c)-1(d), performed on an image near the onset of jamming, illustrate that rigid clusters and regions are closely correlated. This correspondence remains true for our full dataset: Fig. 2(a) is a scatter plot of the measured rigid cluster fraction against the rigid region fraction. All data points are clustered around the diagonal, with no difference between the shear and unshear directions. We find that the pebble game detects a slightly higher rigid fraction at high z, possibly due to boundary effects. This system-scale correspondence carries over to the contact level [Fig. 2(b)], where we compute the adjusted Rand index (ARI) [35,45,46] to measure the bond-scale similarity of the detected clusters/regions. We find ARI > 0(correlation is present), with an average of 0.6 indicating strong positive correlation and some differences again apparent at higher z. This robust [35] high degree of correspondence is significant since the rigid cluster method requires only information about the contact graph

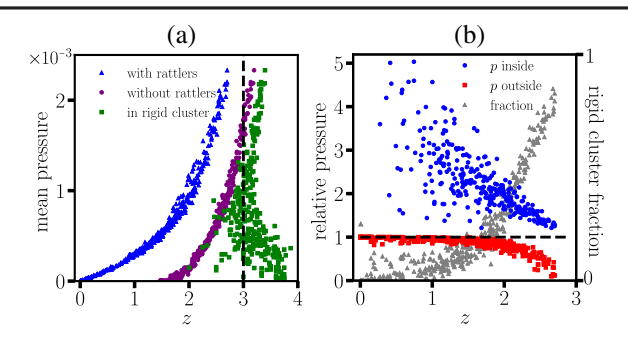


FIG. 3. (a) Mean pressure p as a function of z of the entire packing (blue), within rigid clusters only (green), and with rattlers removed (purple). (b) Pressure inside rigid clusters (blue dots) and outside rigid clusters (red squares) normalized by the mean pressure of the entire packing. The fraction of rigid clusters (gray triangles) is also plotted for reference.

(it is simply a topological measure, only including the classification of sliding vs frictional contacts), in contrast to the explicit displacement computation in the dynamical matrix, which contains the full spatial and mechanical information. The correspondence is not exact, and there are specific (known, but rare) configurations where the two approaches give different results [47]. In Fig. 2(c), we observe that the rigid cluster or region fractions both indicate a continuous transition, and agree with each other within error bars. Using the probability of a spanning rigid cluster (inset), we measure the transition point of $z_c = 2.4 \pm 0.1$. Figure 2(d) shows that the rigid cluster size distribution broadens with increasing z. While our data are limited by finite system size and finite statistics, our distributions do not have a gap, and strongly resemble the results found in simulations of frictional disks [26]. These findings are consistent with a continuous rigidity percolation transition at $z_c < 3$, the mean-field Maxwell criterion with friction. Note that we do not remove rattlers, as they are an integral part of the coexisting floppy and rigid regions and its shear response.

In Fig. 1(d), rigid clusters surround large holes that contain floppy bonds and rattler particles. To characterize these floppy holes, we decompose the rigid cluster graph into a unique set of tiles corresponding to the holes. Each tile is a face of the planar graph where the rigid bonds are the edges connecting vertices at the particle centers. To examine hole statistics, we employ a simple cutoff in hole size h > 2, in units of mean particle area, to exclude (most) simple interstices between particles; the remaining tiles are colored in Fig. 4(a). With increasing z, we observe both more and larger holes [Fig. 4(b)], with the system size as an apparent cutoff in hole size for z > 1.9. We quantify changes in shape using the dimensionless shape parameter $p_0 = P/\sqrt{A}$, where P is the hole perimeter and A is its area; a regular hexagon has $p_0 = 3.72$ and larger values indicate less circular shapes. As z increases, we observe a broader range of shapes with some jaggedness emerging.

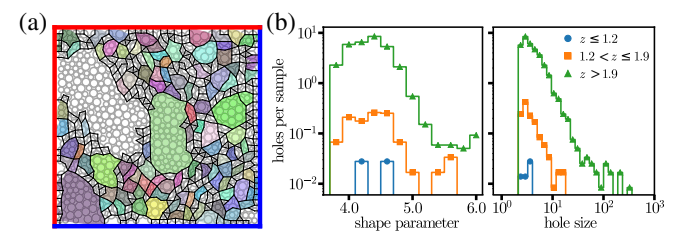


FIG. 4. (a) Rigid clusters (black bonds) decomposed into tiles of closed loops (tile colors are illustrative only; most colored tiles with h > 2 contain nonrigid particles; z = 2.69. (b) Histogram of hole sizes, in units of average particle area and histogram of hole shapes.

Thus, the rigid structures resemble a spongelike porous medium much like the interior of sourdough bread. This finding is compatible with the presence of arch structures, rigid bridges, and hinges linking up rigid clusters to form a spanning network [27], and contrasts with the rigidity transition in frictionless packings, where such floppy holes are not observed [20].

To show that the rigid clusters are mechanically relevant, we calculate the virial pressure p from the contact forces (see Ref. [35]). In Fig. 3(a), we show p(z), rattlers included: the blue curve rises gradually but z remains well below 3. In contrast, we observe that $z \ge 3$ except in some very small clusters when p(z) is calculated within the rigid clusters only. Removing rattlers is not equivalent to identifying the rigid clusters: the same curve p(z) with the rattlers removed, as in Ref. [48], now crosses z=3. In Fig. 3(b), we compute the local pressure inside vs outside the rigid clusters, normalized by p for the entire packing. We find that pressure within rigid clusters is always significantly higher than the mean pressure. In contrast, the pressure in the floppy regions is always below average and drops further for $z \gtrsim 2$, while the mean pressure, the rigid cluster fraction, and the rigid region fraction all start to rise. We interpret Fig. 3 as an emerging rigid backbone, responsible for the rise in pressure and carrying the majority of stress; this same mechanism was previously observed in simulations [26]. In contrast, while we observe anisotropic force chains consistent with shear jamming [11,12], unlike in Ref. [28], we find no correlation between them and the rigid clusters or regions (see Ref. [35]). It therefore remains unclear how the emergence of a rigid backbone and the decomposition into a strong and weak force network [49] fit together.

Discussion.—We have investigated the network structure of real, frictional granular materials under shear using two distinct, but compatible, measures of rigidity. From the probability of finding a spanning rigid cluster, we find a frictional jamming transition at $z_c = 2.4 \pm 0.1$, significantly below z = 3, the lower bound on stable frictional packings given by mean-field constraint counting and also known as random loose packing [50]. Within the

constraints of small system size and limited statistics, we observe a rigid cluster size distribution consistent with a continuous rigidity transition. Our z_c is also lower than simulation results by [28] who observed a rigid spanning cluster at $z_c \approx 2.9$ and the percolation of overconstrained bonds at z=3. Finally, our experimental results contrast with simulations modeling friction with rough, but frictionless particles [51,52].

Open questions include what role the mechanics of these rigid structures plays in local failure under shear. While strong force chains often surround a floppy hole with an arch-like shape, we observed little correlation with pressure: not all forces within floppy regions are weak. Our results need to be complemented with observations of force chains [53–55] and cycles [56] to more completely address rigidity, particularly in the context of shear jamming [11,12]. This could be achieved through topological [57], geometrical [58], or stress-space approaches [59]. Identifying rigid structures will also be important for shear thickening in dense granular suspensions, where a load-bearing rigid cluster abruptly emerges via the exchange of frictionless, lubricated contacts for frictional contacts [60–63].

The data and codes are available on DataDryad [64] and GitHub [34,65].

We thank Arne te Nijenhuis for help collecting photoelastic data, and the James S. McDonnell Foundation (K. E. D., J. E. K.), NSF Grants No. DMR-0644743 (apparatus), No. DMR-1507938, and No. DMR-1832002 (J. M. S.), and BBSRC Grant No. BB/N009150/1-2 (S. H.) for financial support.

- [1] S. Alexander, Phys. Rep. 296, 65 (1998).
- [2] T. C. Lubensky, C. L. Kane, X. Mao, A. Souslov, and K. Sun, Rep. Prog. Phys. 78, 073901 (2015).
- [3] J. C. Maxwell, Philos. Mag. 27, 294 (1864).
- [4] S. Pellegrino and C. R. Calladine, Int. J. Solids Struct. 22, 409 (1986).
- [5] C. S. O'Hern, L. E. Silbert, A. J. Liu, and S. R. Nagel, Phys. Rev. E 68, 011306 (2003).
- [6] M. van Hecke, J. Phys. Condens. Matter 22, 033101 (2009).
- [7] S. Dagois-Bohy, B. P. Tighe, J. Simon, S. Henkes, and M. van Hecke, Phys. Rev. Lett. 109, 095703 (2012).
- [8] C. P. Goodrich, S. Dagois-Bohy, B. P. Tighe, M. van Hecke, A. J. Liu, and S. R. Nagel, Phys. Rev. E 90, 022138 (2014).
- [9] L. E. Silbert, D. Ertaş, G. S. Grest, T. C. Halsey, and D. Levine, Phys. Rev. E 65, 031304 (2002).
- [10] K. Shundyak, M. van Hecke, and W. van Saarloos, Phys. Rev. E 75, 010301(R) (2007).
- [11] D. Bi, J. Zhang, B. Chakraborty, and R. P. Behringer, Nature (London) **480**, 355 (2011).
- [12] Y. Zhao, J. Bars, H. Zheng, J. E. Socolar, and R. P. Behringer, Phys. Rev. Lett. 123, 158001 (2019).
- [13] L. E. Silbert, A. J. Liu, and S. R. Nagel, Phys. Rev. Lett. 95, 098301 (2005).

- [14] E. Somfai, M. van Hecke, W. G. Ellenbroek, K. Shundyak, and W. van Saarloos, Phys. Rev. E 75, 020301(R) (2007).
- [15] S. Henkes, M. van Hecke, and W. van Saarloos, Europhys. Lett. 90, 14003 (2010).
- [16] L. Wenwei, Y. Jin, S. Chen, H. A. Makse, and S. Li, Soft Matter 13, 421 (2017).
- [17] H. Ikeda, C. Brito, M. Wyart, and F. Zamponi, Phys. Rev. Lett. 124, 208001 (2020).
- [18] S. Feng and P. N. Sen, Phys. Rev. Lett. **52**, 216 (1984).
- [19] D. J. Jacobs and B. Hendrickson, J. Comput. Phys. 137, 346 (1997).
- [20] W. G. Ellenbroek, V. F. Hagh, A. Kumar, M. Thorpe, and M. Van Hecke, Phys. Rev. Lett. 114, 135501 (2015).
- [21] D. J. Jacobs and M. F. Thorpe, Phys. Rev. Lett. 75, 4051 (1995).
- [22] D. J. Jacobs and M. F. Thorpe, Phys. Rev. E 53, 3682 (1996).
- [23] D. J. Koeze and B. P. Tighe, Phys. Rev. Lett. 121, 188002 (2018).
- [24] S. Zhang, L. Zhang, M. Bouzid, D. Z. Rocklin, E. Del Gado, and X. Mao, Phys. Rev. Lett. 123, 058001 (2019).
- [25] R. Li and D. Lester, arXiv:2002.00313.
- [26] S. Henkes, D. A. Quint, Y. Fily, and J. M. Schwarz, Phys. Rev. Lett. 116, 028301 (2016).
- [27] K. Liu, S. Henkes, and J. M. Schwarz, Phys. Rev. X 9, 021006 (2019).
- [28] H. A. Vinutha and S. Sastry, Phys. Rev. E **99**, 012123 (2019).
- [29] J. G. Puckett and K. E. Daniels, Phys. Rev. Lett. 110, 058001 (2013).
- [30] E. S. Bililign, J. E. Kollmer, and K. E. Daniels, Phys. Rev. Lett. 122, 038001 (2019).
- [31] K. E. Daniels, J. E. Kollmer, and J. G. Puckett, Rev. Sci. Instrum. 88, 051808 (2017).
- [32] A. Abed Zadeh et al., Granular Matter 21, 83 (2019).
- [33] H. Zheng, J. A. Dijksman, and R. P. Behringer, Europhys. Lett. **107**, 34005 (2014).
- [34] J. E. Kollmer, Photo-Elastic Granular Solver (PEGS), https://github.com/jekollmer/PEGS.
- [35] See Supplemental Material at http://link.aps.org/supplemental/10.1103/PhysRevLett.126.088002 for details of our methods, including the robustness of experimental contact detection, the pebble game algorithm, constructing a dynamical matrix to identify rigid regions, parameter choices for the analysis, the adjusted rand index, and finally our comparison to shear jamming.
- [36] For the slowly sheared simulations of Ref. [26], as observed by S. H.
- [37] G. Laman, J. Eng. Math. 4, 331 (1970).
- [38] B. Servatius and H. Servatius, *Rigidity Theory and Applications*, edited by M. F. Thorpe and P. M. Duxbury (Kluwer Academic/Plenum Publishers, New York, 1999).
- [39] T.-S. Tay, J. Comb. Theory Ser. B 36, 95 (1984).
- [40] P. A. Cundall and O. D. L. Strack, Géotechnique **29**, 47 (1979).
- [41] N. Ashcroft and N. Mermin, Solid State Physics (Saunders College, Philadelphia, 1976).
- [42] A. J. Liu and S. R. Nagel, Annu. Rev. Condens. Matter Phys. 1, 347 (2010).

- [43] K. L. Johnson, *Contact Mechanics* (Cambridge University Press, Cambridge, England, 1985).
- [44] J. Irving and J. G. Kirkwood, J. Chem. Phys. 18, 817 (1950).
- [45] W. M. Rand, J. Am. Stat. Assoc. 66, 846 (1971).
- [46] L. Hubert and P. Arabie, J. Classif. 2, 193 (1985).
- [47] D. R. Lester and R. Li, J. Comput. Phys. **369**, 225 (2018).
- [48] T. Majmudar, M. Sperl, S. Luding, and R. P. Behringer, Phys. Rev. Lett. 98, 058001 (2007).
- [49] F. Radjai, D. E. Wolf, M. Jean, and J.-J. Moreau, Phys. Rev. Lett. 80, 61 (1998).
- [50] G. Y. Onoda and E. G. Liniger, Phys. Rev. Lett. 64, 2727 (1990).
- [51] S. Papanikolaou, C. S. O'Hern, and M. D. Shattuck, Phys. Rev. Lett. 110, 198002 (2013).
- [52] M. Wyart, S. R. Nagel, and T. A. Witten, Europhys. Lett. 72, 486 (2005).
- [53] C.-H. Liu, S. R. Nagel, D. A. Schecter, S. N. Coppersmith, S. Majumdar, O. Narayan, and T. A. Witten, Science 269, 513 (1995).
- [54] D. Howell, R. P. Behringer, and C. Veje, Phys. Rev. Lett. 82, 5241 (1999).

- [55] K. P. Krishnaraj and P. R. Nott, Phys. Rev. Lett. 124, 198002 (2020).
- [56] A. Tordesillas, D. M. Walker, and Q. Lin, Phys. Rev. E 81, 011302 (2010).
- [57] C. Giusti, L. Papadopoulos, E. T. Owens, K. E. Daniels, and D. S. Bassett, Phys. Rev. E 94, 032909 (2016).
- [58] J. M. Rieser, C. P. Goodrich, A. J. Liu, and D. J. Durian, Phys. Rev. Lett. 116, 088001 (2016).
- [59] S. Sarkar, D. Bi, J. Zhang, J. Ren, R. P. Behringer, and B. Chakraborty, Phys. Rev. E 93, 042901 (2016).
- [60] M. Wyart and M. E. Cates, Phys. Rev. Lett. 112, 098302 (2014).
- [61] R. Mari, R. Seto, J. F. Morris, and M. M. Denn, Proc. Natl. Acad. Sci. U.S.A. 112, 15326 (2015).
- [62] J. E. Thomas, K. Ramola, A. Singh, R. Mari, J. F. Morris, and B. Chakraborty, Phys. Rev. Lett. 121, 128002 (2018).
- [63] M. Gameiro, A. Singh, L. Kondic, K. Mischaikow, and J. F. Morris, Phys. Rev. Fluids 5, 034307 (2020).
- [64] K. Liu et al., Dryad, Dataset, https://doi.org/10.5061/dry-ad.d51c5b01k.
- [65] S. Henkes, Rigid Library, https://github.com/silkehenkes/ RigidLibrary.